AMERICAN SOCIETY FOR MICROBIOLOGY | mBio®

RESEARCH ARTICLE

CLAG3 Self-Associates in Malaria Parasites and Quantitatively Determines Nutrient Uptake Channels at the Host Membrane

Ankit Gupta,[a] Praveen Balabaskaran-Nina,[a]* Wang Nguitragool,[a]* Gagandeep S. Saggu,[a] Marc A. Schureck,[a] Sanjay A. Desai[a]

[a]Laboratory of Malaria and Vector Research, NIAID, National Institutes of Health, Rockville, Maryland, USA

ABSTRACT Malaria parasites increase host erythrocyte permeability to ions and nutrients via a broad-selectivity channel known as the plasmodial surface anion channel (PSAC), linked to parasite-encoded CLAG3 and two associated proteins. These proteins lack the multiple transmembrane domains typically present in channel-forming proteins, raising doubts about their precise roles. Using the virulent human *Plasmodium falciparum* parasite, we report that CLAG3 undergoes self-association and that this protein's expression determines channel phenotype quantitatively. We overcame epigenetic silencing of *clag3* paralogs and engineered parasites that express two CLAG3 isoforms simultaneously. Stoichiometric expression of these isoforms yielded intermediate channel phenotypes, in agreement with observed trafficking of both proteins to the host membrane. Coimmunoprecipitation and surface labeling revealed formation of CLAG3 oligomers. *In vitro* selections applied to these transfectant lines yielded distinct mutants with correlated changes in channel activity. These findings support involvement of the identified oligomers in PSAC formation and parasite nutrient acquisition.

IMPORTANCE Malaria parasites are globally important pathogens that evade host immunity by replicating within circulating erythrocytes. To facilitate intracellular growth, these parasites increase erythrocyte nutrient uptake through an unusual ion channel. The parasite CLAG3 protein is a key determinant of this channel, but its lack of homology to known ion channels has raised questions about possible mechanisms. Using a new method that allows simultaneous expression of two different CLAG3 proteins, we identify self-association of CLAG3. The two expressed isoforms faithfully traffic to and insert in the host membrane, while remaining associated with two unrelated parasite proteins. Both the channel phenotypes and molecular changes produced upon selections with a highly specific channel inhibitor are consistent with a multiprotein complex that forms the nutrient pore. These studies support direct involvement of the CLAG3 protein in channel formation and are relevant to antimalarial drug discovery projects targeting parasite nutrient acquisition.

KEYWORDS *Plasmodium falciparum*, host-pathogen interactions, integrase, ion channels, malaria, molecular biology, multiprotein complexes, nutrient transport

Plasmodium spp. infect a broad range of vertebrates and cause malaria in humans. These parasites evade host immune responses by invasion, growth, and asexual replication within circulating erythrocytes. The most virulent human pathogen, *Plasmodium falciparum*, remodels the host erythrocyte for its own benefit by exporting many proteins into the host cytosol, altering host cell deformability and cytoadherence, and increasing erythrocyte permeability to nutrients and other solutes (1–3).

Forward and reverse genetic screens along with pharmacological studies have recently determined that the increased permeability of nearly all solutes results from a single ion channel termed the plasmodial surface anion channel (PSAC); these studies linked PSAC to the *clag* multigene family conserved in all examined malaria parasites

Received 14 February 2018 **Accepted** 10 April 2018 **Published** 8 May 2018

Citation Gupta A, Balabaskaran-Nina P, Nguitragool W, Saggu GS, Schureck MA, Desai SA. 2018. CLAG3 self-associates in malaria parasites and quantitatively determines nutrient uptake channels at the host membrane. mBio 9:e02293-17. https://doi.org/10.1128/mBio.02293-17.

Editor L. David Sibley, Washington University School of Medicine

Address correspondence to Sanjay A. Desai, sdesai@niaid.nih.gov.

* Present address: Praveen Balabaskaran-Nina, Department of Epidemiology and Public Health, Central University of Tamil Nadu, Thiruvarur, India; Wang Nguitragool, Department of Molecular Tropical Medicine and Genetics, Mahidol University, Bangkok, Thailand.

(4–9). Two unrelated but also conserved proteins, RhopH2 and RhopH3, associate with CLAGs and are also essential for PSAC activity (10–13).

While these molecular studies have convincingly implicated these parasite genes in nutrient uptake, fundamental questions remain about how the encoded proteins determine PSAC activity and the importance of increased permeability to intracellular parasite development. CLAG3.1 and CLAG3.2, related paralogs encoded by chromosome 3 in *P. falciparum*, are exported to the host membrane, where they are integral and susceptible to extracellular protease treatment (14). Nevertheless, the absence of unambiguous transmembrane domains and the lack of homology to known ion channels casts doubt on whether CLAG3 can form an ion channel pore. While association with RhopH2 and RhopH3 might facilitate pore formation, these other proteins do not appear to be exposed at the host cell surface (11). Molecular studies to define the role of CLAG3 have been complicated by epigenetic silencing, which allows infected cells to express only one *clag3* paralog for several generations before switching to the other paralog (15, 16). While these two genes encode proteins that are 90 to 95% identical, a short polymorphic motif is exposed at the erythrocyte surface and may affect function (8). This epigenetic switching confounds DNA transfection studies designed to examine channel phenotypes. Yet another difficulty is *clag3*'s large size, which complicates full gene replacements through technologies such as CRISPR-Cas9.

Here, we overcame these problems by introducing a silent *attB* site in the last *clag3* intron, allowing facile integrations through a novel application of Bxb1 integrase transposition technology. This not only allowed the efficient replacement of the downstream open reading frame (ORF) but permitted constitutive expression of two distinct CLAG3 isoforms at stoichiometric levels within individual parasites. Simultaneous expression of two isoforms yielded transport with intermediate properties. Pull-down experiments detected specific CLAG3 oligomerization, suggesting formation of an aqueous pore. We also used the resulting parasite as well as a distinct merodiploid parasite produced through random *piggyBac* insertional mutagenesis to examine how parasite cultures respond to selective pressure against individual CLAG3 isoforms. The molecular changes identified through these selections indicate that the intracellular parasite requires channel-mediated nutrient uptake and help define the roles served by these proteins. Our studies support direct involvement of CLAG3 in formation of PSAC, an essential nutrient uptake channel.

RESULTS

An intronic *attB* site facilitates production of tandem CLAG3 isoforms with separate epitope tags. While most lab and field isolates have two *clag3* genes under epigenetic control (referred to as *clag3.1* and *clag3.2* [4, 7, 10, 15]), some parasites have a single hybrid copy termed *clag3h* formed by crossover homologous recombination to yield copy number reduction (17). The KC5 parasite line carries a single *clag3h* gene and was chosen for our transfections to simplify interpretation; in KC5, the crossover occurred between conserved polymorphisms located 607 and 844 bp from the start of *clag3h*, with the 5′ end derived from *clag3.2* and the majority of the gene derived from an ancestral *clag3.1* (see Fig. S1 in the supplemental material). We first introduced a silent *attB* site into the last intron of the *clag3h* gene by single homologous recombination (Fig. 1A). To facilitate preferential recombination upstream of this intron, the transfection plasmid carried a recodonized last exon whose product matches that of the *clag3.1* gene from the Dd2 laboratory line (sLE_{Dd2} [Fig. S2A] in the supplemental material). PCR confirmed integration of this plasmid in the *C3attB* limiting dilution clone (Fig. S2B); DNA sequencing confirmed the expected introduction of the *attB* element flanked by intronic sequences with canonical splice sites. Immunoblotting revealed that the transfectant produces a CLAG3 protein of unchanged size (Fig. 1B). We then quantified PSAC activity by tracking osmotic lysis of infected cells in sorbitol (red trace, Fig. 1C), a sugar alcohol taken up primarily via the CLAG3-associated PSAC. A statistically insignificant increase in the osmotic lysis halftime indicates preserved sorbitol

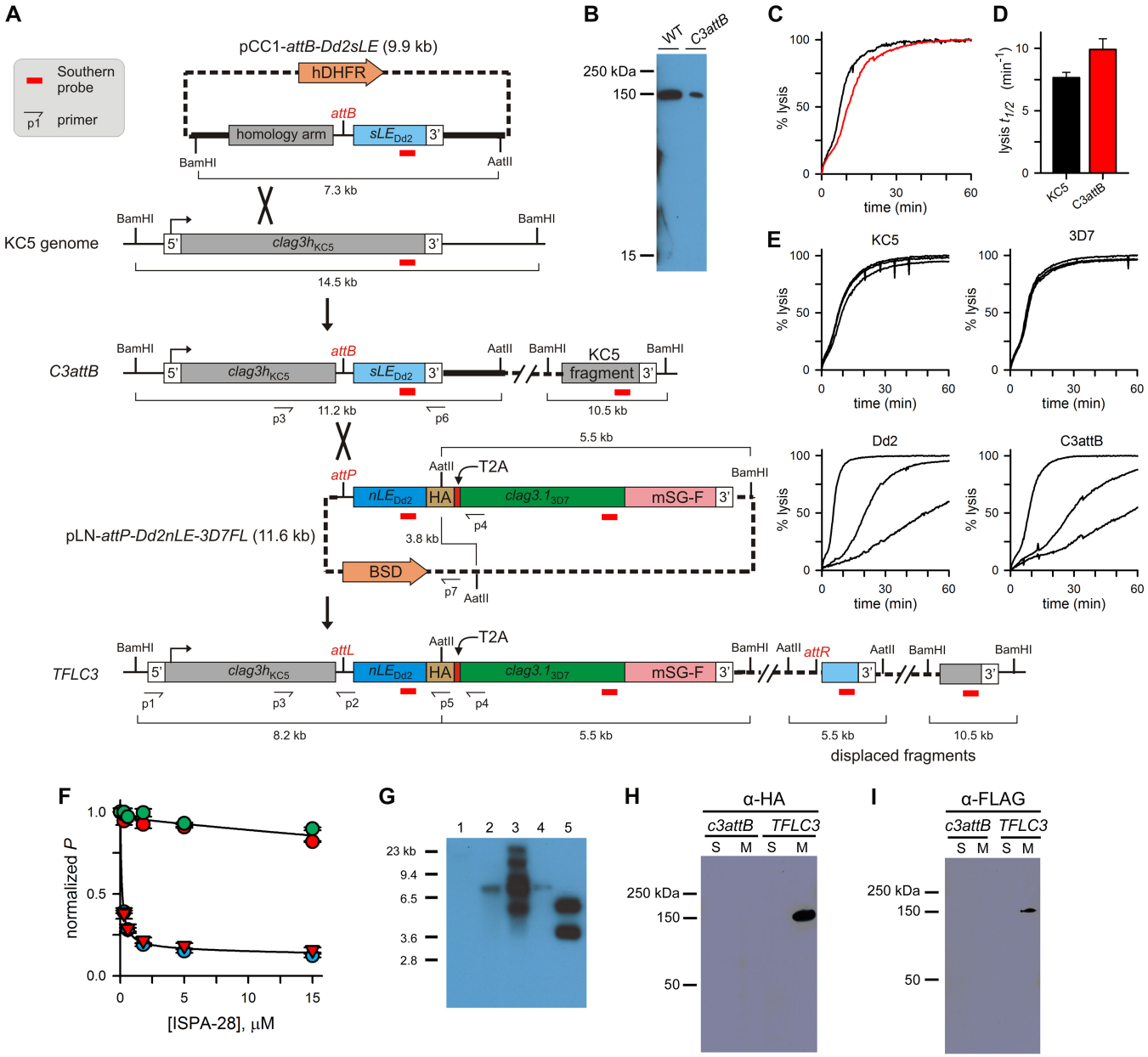

FIG 1 Intronic *attB* as a strategy for rapid introduction of complex gene modifications. (A) Schematic showing transfection approach. The *attB* was introduced into wild-type KC5 by homologous recombination to produce the *C3attB* parasite; a second transfection using Bxb1 integrase yielded the *TFLC3* clone. The tandem Dd2 and 3D7 CLAG3 isoforms are expressed under the native KC5 *clag3h* promoter and separated during translation due to the T2A skip peptide. After transfection, the Dd2 isoform carries a C-terminal HA tag, while the 3D7 isoform carries a larger miniSOG-FLAG tag (labeled mSG-F). Selectable markers, human dihydrofolate reductase (hDHFR) and blasticidin-S deaminase (BSD), are shown with orange arrows; relevant restriction sites and fragment sizes are shown. (B) Immunoblotting of total cell lysates from KC5 and *C3attB* lines, probed with mouse polyclonal anti-CLAG3. WT, wild type. (C) Sorbitol-induced osmotic lysis kinetics for KC5 and *C3attB* (black and red traces, respectively). (D) Mean ± SEM lysis halftimes for these lines. (E) Osmotic lysis kinetics for indicated parasites with addition of 0, 0.6, and 15 μM ISPA-28 (top to bottom traces in each panel, respectively). Note the dose-dependent inhibition in the Dd2 and *C3attB* parasites. (F) Mean ± SEM permeability in ISPA-28 dose-response experiments as in panel E for wild-type KC5, 3D7, and Dd2 (red, green, and blue circles, respectively) and the *C3attB* transfectant parasite (red triangles). Solid lines represent fits to $y = \{a/[1 + (x/c)]\} + \{(1 - a)/[1 + (x/b)]\}$, where *a*, *b*, and *c* are constants. ISPA-28 block in *C3attB* matches that of Dd2. (G) Southern blotting confirms integration in *C3attB* and *TFLC3* parasite genomes. Hybridization was performed with a mixed probe as marked in panel A. Lanes: 1, wild-type KC5 genome; 2, *C3attB* genome; 3, *TFLC3* genome; 4, pCC1-attB-Dd2sLE plasmid; 5, pLN-attP-Dd2nLE-3D7FL plasmid; an additional larger band (>23 kb) in *TFLC3* may reflect undigested concatemers formed by integrase-mediated recombination of *attP*- and *attB*-containing plasmids. Please see Fig. S2D for increased exposure to allow detection of bands in lanes 1 and 2. (H and I) Immunoblot assays using indicated epitope tag antibodies. *TFLC3* expresses both the Dd2-HA-tagged and the 3D7-miniSOG-FLAG-tagged CLAG3 proteins. S and M represent soluble and membrane-associated fractions, respectively, from Percoll-enriched trophozoite-infected cells.

permeability (Fig. 1D; P = 0.09, *n* = 5 to 9 each) and indicates that the silent *attB* element is not detrimental.

We predicted that replacement of the KC5 C-terminal sequence with the Dd2 *clag3.1* last exon would produce channels inhibited by ISPA-28, a Dd2-specific inhibitor that enabled genetic mapping of PSAC phenotypes to *clag3* (4, 5). This prediction is based on the observation that inherited polymorphisms account for the specific action on Dd2 CLAG3.1 and that most of the polymorphisms are within a 10- to 30-residue motif encoded by the last exon. This hypervariable region (HVR) is exposed at the host erythrocyte surface (14). Consistent with our prediction, ISPA-28 potently blocked channels on *C3attB* but had negligible effect on uptake by wild-type KC5 parasites (Fig. 1E). Channels from the untransfected 3D7 parasite are also not blocked; while both KC5 and 3D7 carry genes that resemble Dd2 *clag3.1*, they have distinct HVR sequences. Dose-response studies revealed that the ISPA-28 block in *C3attB* matches that of untransfected Dd2 parasites (Fig. 1F). Thus, the last exon of *clag3* is sufficient to fully define channel block and binding affinity for ISPA-28; these findings implicate the unique HVR sequence of Dd2 CLAG3.1 in ISPA-28 binding and block.

The silent *attB* introduced into the last intron should enable rapid transfection to insert distal epitope tags and regulatory elements. As proof of principle, we found that a C-terminal hemagglutinin (HA) epitope tag could be readily added (Fig. S3). To explore whether more-complex sequences can be inserted at this site, we designed and performed a transfection to allow simultaneous expression of tandem full-length *clag3* isoforms under the control of the endogenous KC5 *clag3h* promoter (Fig. 1A). The pLN-attP-Dd2nLE-3D7FL plasmid consists of the *attP* sequence required for recombination with the genomic *attB* site, the distal intronic sequence, the native Dd2 *clag3.1* last exon with a C-terminal HA tag, an in-frame viral T2A ribosome skip peptide, and a full-length 3D7 *clag3.1* cDNA terminated with tandem miniSOG and FLAG epitope tags (18). Although the two *clag3* genes are large (5.2 kb each) and we sought epitope tags of distinct sizes on the two isoforms, the compact design and use of *attB-attP* recombination allowed synthesis of a manageable transfection plasmid of 11.6 kb size (Fig. 1A). Successful integration and transcription by the native *clag3h* promoter should yield bicistronic expression of two distinct CLAG3 isoforms because the T2A skip peptide functions to cleave the nascent protein into two polypeptides during translation (19). This strategy is designed to allow simultaneous expression of two distinct CLAG3 isoforms, which is normally prevented by epigenetic silencing and monoallelic expression.

After this second transfection and limiting dilution, we obtained the *TFLC3* clone (for "tandem full-length *clag3*") with the expected integration (Fig. S2C). Southern blotting with a probe mixture designed to interact promiscuously with all *clag3* sequences yielded a single band in KC5, a smaller band that reflects two digested fragments of nearly equal size in *C3attB*, and multiple bands corresponding to 4 distinct sites of probe hybridization after the second transfection (Fig. 1G and increased-exposure blot in Fig. S2D). Immunoblotting with antibodies to the HA and FLAG epitope tags identified the expected addition of both tags through a single transfection (Fig. 1H and I). These large proteins were faithfully separated at the viral T2A skip peptide, yielding bands consistent with their calculated sizes (163 and 171 kDa for the tagged Dd2 and 3D7 isoforms, respectively); an ~330-kDa band indicative of uncleaved fusion protein was not detected, suggesting efficient ribosome skipping at the T2A sequence and/or rapid degradation of residual fusion protein. Finally, both CLAG3 isoforms fractionated to the membrane pellet upon ultracentrifugation, as previously demonstrated for native CLAG3 (4).

Our transfection strategy predicted that *TFLC3* parasites will simultaneously express the two CLAG3 isoforms under a single *clag3h* promoter. Indirect immunofluorescence microscopy indeed revealed that each infected cell was recognized by both anti-HA and anti-FLAG antibodies (Fig. 2A). In schizont-infected cells, the two proteins colocalized as discrete puncta within developing merozoites (Fig. 2A, top row), consistent with CLAG3 packaging into apical rhoptry organelles (20). As observed for CLAG3 and other

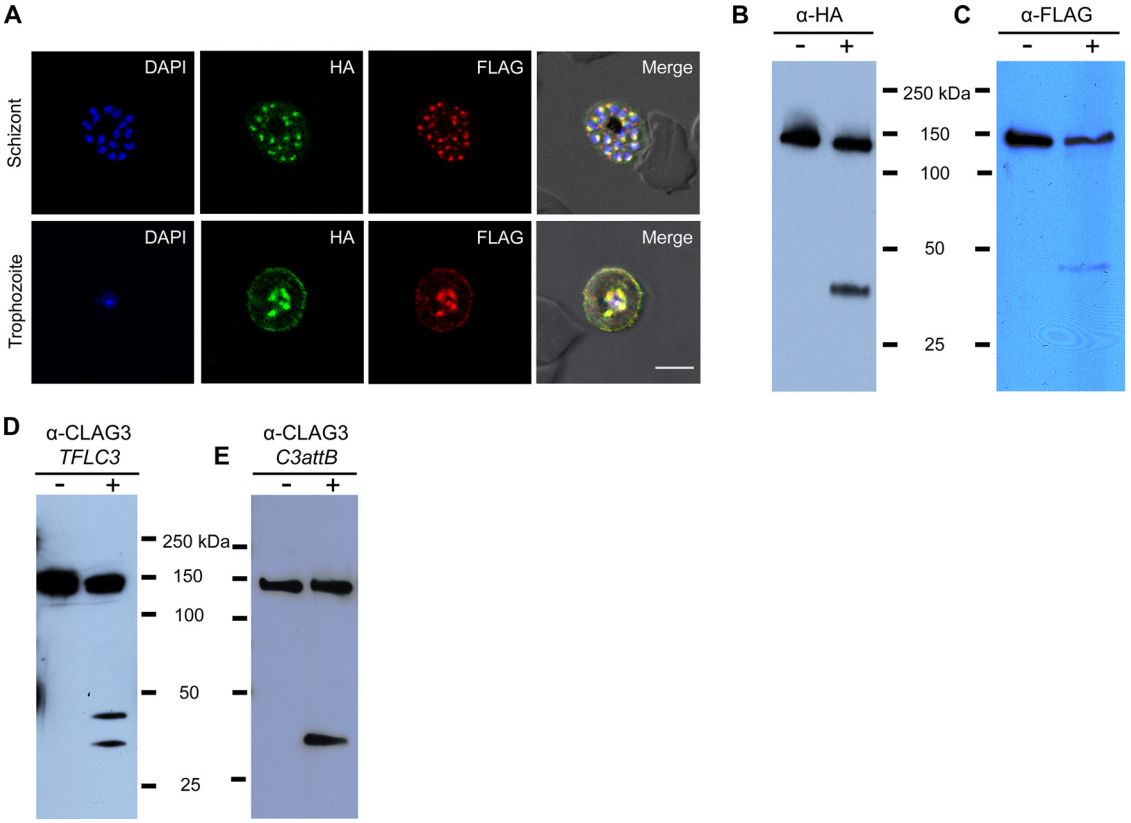

FIG 2 Coexpression and faithful trafficking of tandem CLAG3 isoforms. (A) Indirect immunofluorescence images showing colocalization of Dd2-HA and 3D7-miniSOG-FLAG CLAG3 isoforms in *TFLC3* parasites at the schizont stage and in trophozoites after invasion of new erythrocytes. Bar, 5 μm. (B and C) Immunoblot assays performed using *TFLC3* cell lysates and indicated epitope tag antibodies without or with extracellular pronase E treatment prior to cell lysis (− and +, respectively). (D and E) Immunoblot assays using anti-CLAG3 antibody and indicated parasites, without and with pronase E treatment (− and +, respectively). While two cleavage products are detected in *TFLC3*, the *C3attB* parent produces a single fragment.

rhoptry proteins (11), both isoforms were transferred to new erythrocytes after egress and reinvasion at the end of the intracellular cycle. Upon maturation of these daughter parasites to the trophozoite stage (Fig. 2A, bottom row), both isoforms were observed to be exported into host cytosol and again colocalized at the cell periphery, suggesting association with the erythrocyte membrane.

Because proteolysis within its extracellular HVR is the hallmark of the CLAG3 pool integral to the host membrane (14), we then performed immunoblotting after extracellular protease treatment and found that both CLAG3 isoforms are integral at the host membrane in *TFLC3*. Pronase E yielded proteolytic fragments of 35 to 45 kDa in size when probed with antibodies to the HA and FLAG epitope tags present on the Dd2 and 3D7 isoforms, respectively (Fig. 2B and C). Importantly, while immunoblotting with the *C3attB* parent produced a single cleavage product when probed with a polyclonal antibody to the conserved CLAG3 C terminus (4), *TFLC3* produced two cleavage products (Fig. 2D and E). The distinct sizes of these two products were anticipated by our transfection strategy because of the differing C-terminal epitope tags added to the two CLAG3 isoforms. A 7.3-kDa-larger size for the tagged 3D7 isoform is predicted based on protease-mediated cleavage at the distal ends of each CLAG3 HVR domain, the tandem miniSOG and FLAG epitope tag molecular weights, and the segregation site within the T2A skip peptide (19). Although this difference in size could not be easily confirmed for the full-length CLAG3 isoforms, it is apparent for the two protease-induced cleavage products because of clearly resolved migration of the smaller C-terminal fragments (Fig. 2D).

CLAG3 isoforms interact with each other in stable complexes. We next explored interactions between the two CLAG3 isoforms using coimmunoprecipitation (co-IP)

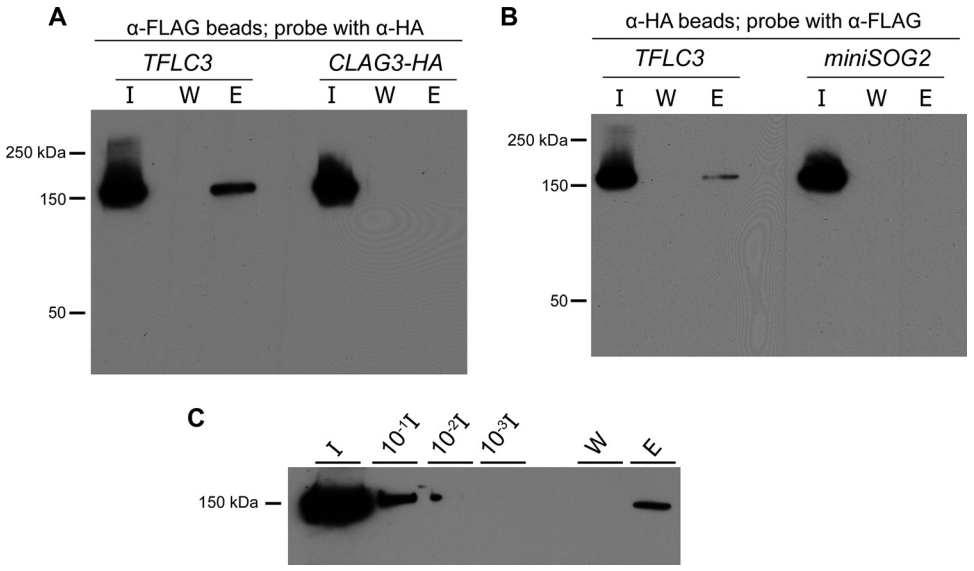

FIG 3 CLAG3 oligomerizes at the host erythrocyte membrane. (A) Coimmunoprecipitation of lysates from indicated parasites using anti-FLAG beads and an anti-HA probe. Lanes show solubilized input (I), final wash (W), and eluate (E). (B) Similar coimmunoprecipitations using anti-HA beads and an anti-FLAG probe. (C) Fraction of CLAG3 in hetero-oligomers, quantified by comparison of the eluate to serial dilutions of the input. The eluate band is more intense than a 100× dilution of the input (10^{-2}I).

experiments. Pulldown using anti-FLAG beads and the *TFLC3* parasite revealed a stable association between the FLAG-tagged 3D7 CLAG3 protein and the HA-tagged Dd2 CLAG3 protein (Fig. 3A). A control transfectant (*CLAG3-HA*), also made using KC5 parasites to introduce an HA-tagged Dd2 *clag3.1* terminal sequence but without a FLAG-tagged bait protein (Fig. S4A), did not yield detectable protein in pulldowns, excluding nonspecific binding of HA-tagged CLAG3 to anti-FLAG beads under our conditions. The reverse co-IP experiment using anti-HA beads confirmed the association in *TFLC3*, as the FLAG-tagged 3D7 allele could also be pulled down (Fig. 3B). Here, a separate control transfectant expressing these two CLAG3 alleles but without HA tagging of the Dd2 allele, *miniSOG2* (Fig. S4B to D), excluded nonspecific binding of either the FLAG tag or the 3D7 isoform to anti-HA beads. These experiments confirmed a stable association between the two CLAG3 isoforms and implicate formation of CLAG3 hetero-oligomers within trophozoites.

Previous imaging and cell fractionation experiments have revealed distinct subcellular pools of CLAG3 within maturing trophozoites that presumably reflect protein in transit to the host membrane (11, 21). As CLAG3 monomers may self-associate at only some of these sites, we next used immunoblotting to estimate the fraction of HA-tagged protein that is coprecipitated on anti-FLAG beads in *TFLC3*. By comparison to serial dilutions of the input lysate and measurement of band intensities, we estimated that between 1 and 10% of the HA-tagged Dd2 isoform is in stable association with the FLAG-tagged 3D7 CLAG3 protein (Fig. 3C). Because this experiment identifies only complexes that contain at least one copy of each CLAG3 isoform, it likely underestimates the fraction of HA-tagged protein in oligomers; the actual value will depend on whether the two isoforms assort randomly into oligomers and the presently unknown number of monomers in each membrane complex. CLAG3 self-association may be further underestimated if our detergent and immunoprecipitation conditions compromise the integrity of protein complexes.

We also performed blue native PAGE (BN-PAGE) experiments to examine formation of complexes containing more than one CLAG3 monomers but found that BN-PAGE conditions yield anomalous migration of these proteins. *n*-Dodecyl β-D-maltoside (DDM) or a low 0.05% concentration of FC-12 detected CLAG3 within a high-molecular-weight complex that migrated near the 720-kDa marker (Fig. S5A); a similar band

detected when probing for RhopH3 suggests that this represents the intact RhopH complex (Fig. S5B). Addition of SDS, a denaturing detergent, to either of these samples disrupted the complex and yielded a single CLAG3 band migrating near the 480-kDa marker. Increasing the FC-12 concentration to 1% also disrupted the complex and yielded similar CLAG3 migration; addition of SDS to this sample did not further increase mobility. Thus, this band likely represents a CLAG3 monomer that migrates at 400 to 500 kDa instead of 160 kDa as expected from its gene model; RhopH3 also exhibited anomalous migration in BN-PAGE (Fig. S5B), as has been observed for many membrane-associated proteins (22). SDS-PAGE followed by silver staining also suggested that 1% FC-12 disrupts the complex, as CLAG3 could not coimmunoprecipitate either RhopH2 or RhopH3 from total cell lysates, whereas these proteins were readily recovered in experiments using 1% DDM (Fig. S5C). Finally, coimmunoprecipitation (co-IP) using the *TFLC3* merodiploid parasite after solubilization with 1% FC-12 revealed that the FLAG and HA isoforms did not remain associated (Fig. S5D), in contrast to the results with either Triton X-100 or DDM. Each of these observations confirms that 1% FC-12 denatures the RhopH complex and that CLAG3 migration is anomalous in BN-PAGE. In light of these findings, caution is required in interpreting the recent proposal of CLAG3 homotrimers based solely on FC-12 solubilization and the apparent molecular weight in BN-PAGE (23). Co-IP using *TFLC3* parasites expressing two CLAG3 isoforms, as we have used here (Fig. 3), provides more direct experimental evidence supporting CLAG3 self-association.

Both CLAG3 isoforms contribute to PSAC-mediated nutrient uptake. The tandem CLAG3 isoforms expressed in *TFLC3* are separated into two proteins during translation, and traffic to the host membrane; our co-IPs suggest that they assemble into complexes containing two or more CLAG3 monomers, presumably still in association with other RhopH proteins. Depending on subunit stoichiometries and random assortment into aggregates containing the tagged Dd2 and 3D7 CLAG3 isoforms, we propose that there may be at least three distinct complexes at the host cell surface in *TFLC3* (Fig. 4A). To explore this model and how these complexes contribute to formation of functional channels, we next measured organic solute uptake and quantified block by ISPA-28, an inhibitor specific for the Dd2 CLAG3.1 isoform. While this blocker potently inhibits sorbitol uptake by cells infected with Dd2 parasites ($K_{0.5}$ of 56 $\pm$ 5 nM [4]), it has negligible activity against PSAC associated with 3D7 parasites (Fig. 1E and 4B, $K_{0.5} > 15$ μM). Importantly, *TFLC3* produced PSAC activity intermediate between these two wild-type parasites (Fig. 4B and F), indicating that each of the isoforms is functional at the host membrane.

We next examined CLAG3 trafficking and channel phenotype using the *miniSOG2* parasite, which is also a CLAG3 merodiploid parasite that instead expresses the Dd2 and 3D7 isoforms under separate promoters (Fig. 4C and S4B to D). Because this parasite was generated using *piggyBac* transfection (24), the 3D7 CLAG3 isoform is expressed from a distinct genomic site after transposase-mediated integration of the inverted terminal repeat (ITR) cassette. Southern blotting confirmed a single integration event without residual episomes in the *miniSOG2* clone (Fig. S4D). In this parasite, the 3D7 allele carried the same tandem miniSOG-FLAG epitope tag at its C terminus as in *TFLC3* but with expression under a heterologous *msp2* promoter. We selected this promoter because *msp2* exhibits a stage-specific transcription profile similar to that of *clag* genes in *P. falciparum* (25). This choice yielded CLAG3 expression and faithful trafficking to the rhoptry within schizonts and export to the host compartment in trophozoites (Fig. 4D). Despite use of a heterologous promoter and expression from a distinct genomic locus, the tagged 3D7 isoform successfully integrated at the host membrane, as confirmed by susceptibility to extracellular protease (Fig. 4E). As observed with *TFLC3*, this merodiploid also produced two cleavage products when probed with anti-CLAG3 antibody (Fig. 4F) and an intermediate ISPA-28 inhibition phenotype (Fig. 4B and G). Thus, CLAG3 protein contribution to channel-mediated solute uptake does not depend on genomic site, the specific promoter used, or polypeptide separation within the T2A linker.

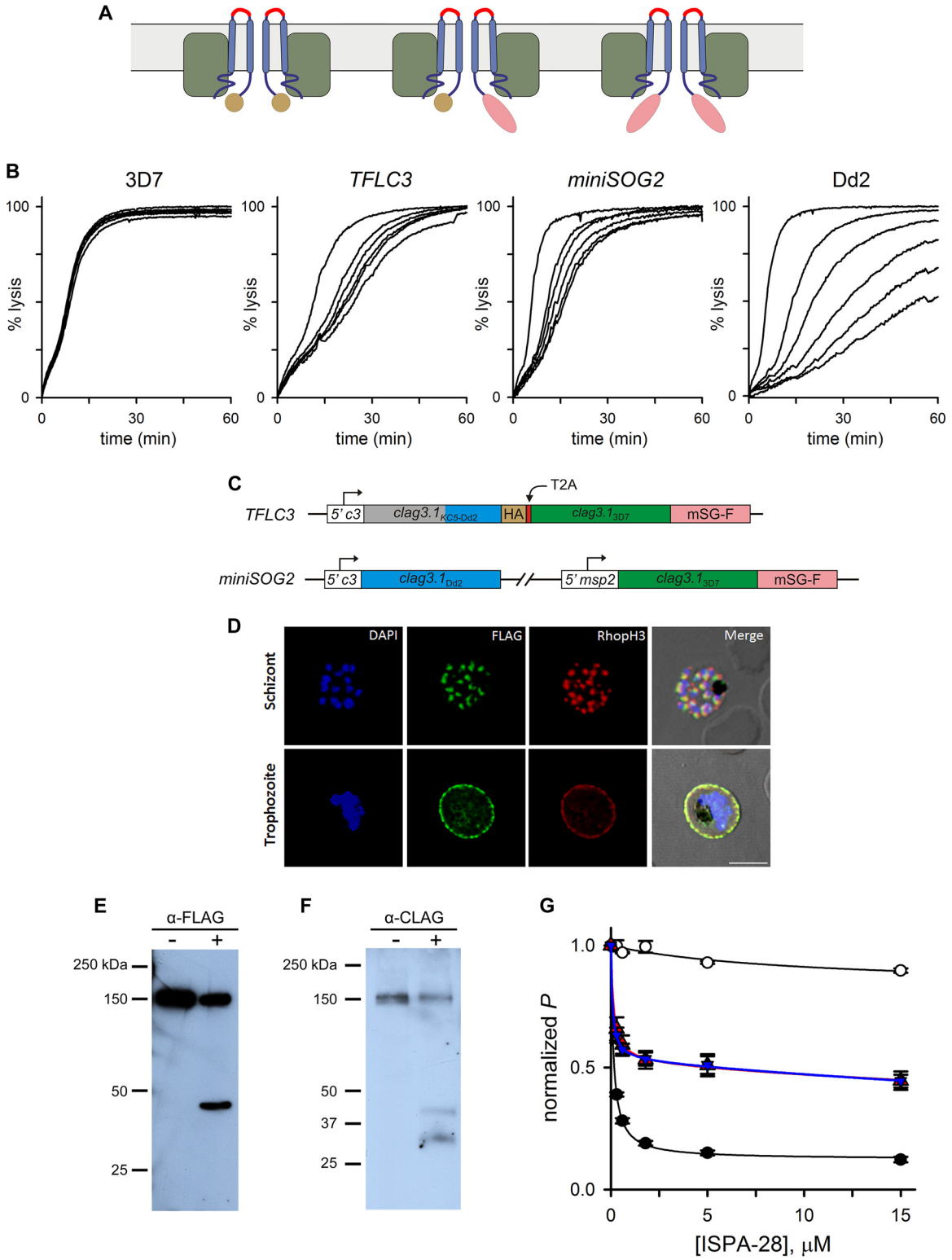

FIG 4 CLAG3 merodiploids reveal a stoichiometric contribution to PSAC-mediated nutrient uptake. (A) Schematic showing the minimum distinct combinations of host membrane RhopH complexes in the *TFLC3* parasite. CLAG3 is shown as blue ribbon dimers embedded in the host membrane; note the permutations of the two C-terminal epitope tags (gold circles and pink ellipses). RhopH2 and RhopH3 are represented in green. (B) Sorbitol uptake kinetics for indicated parasites with addition of 0, 0.3, 0.6, 1.8, 5, and 15 μM ISPA-28 (top to bottom traces in each panel, respectively). Inhibition in *TFLC3* and *miniSOG2* is intermediate between those observed for 3D7 and Dd2. (C) Ribbon diagrams showing expression of two CLAG3 isoforms in *TFLC3* and *miniSOG2*. (D) Immunofluorescence images showing trafficking of the 3D7-miniSOG-FLAG CLAG3 isoform in *miniSOG2*. This protein, expressed under the *msp2* promoter, colocalizes with RhopH3 in schizonts and is exported normally in trophozoites after invasion of new erythrocytes. Bar, 5 μm. (E and F) Immunoblot assays

(Continued on next page)

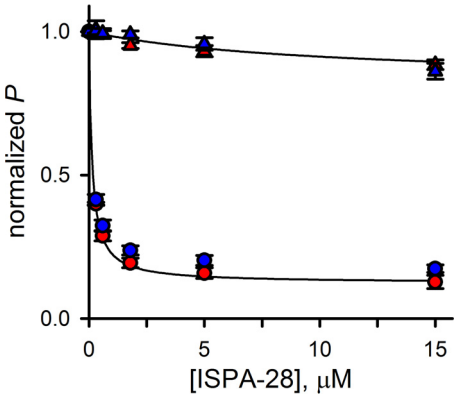

FIG 5 *In vitro* selections revert channel phenotypes to those of parental lines. Dose responses for PSAC inhibition by ISPA-28 after selections applied to *TFLC3* or *miniSOG2* (blue and red symbols, respectively). Circles represent clones generated after treatment with sorbitol, and ISPA-28; triangles reflect clones obtained after cultivation in PGIM with this inhibitor. These clones exhibit potencies that match those of Dd2 or 3D7 (reflected by the solid lines, reproduced from the best fits in Fig. 4G).

Notably, the ISPA-28 susceptibilities of *miniSOG2* and *TFLC3* parasites were indistinguishable ($P = 0.97$ at 15 μM inhibitor, $n = 12$ to 14 trials each). Thus, findings with two distinct merodiploid parasites suggest that the identified CLAG3 oligomers are physiologically significant.

***In vitro* selections against CLAG3 merodiploids: phenotype changes linked to distinct gene modifications.** In contrast to their expression in *TFLC3* and *miniSOG2*, the two *clag3* genes in most wild-type parasites exhibit monoallelic expression through epigenetic control (8), yielding two subpopulations expressing one or the other allele (4). As predicted for subpopulations in steady-stage cultures, ISPA-28 has been previously used for purifying selections either for or against cells expressing the Dd2 *clag3.1* isoform. Positive selection for this isoform has been demonstrated with brief daily incubations in sorbitol with ISPA-28 to produce osmotic lysis of cells that express *clag3* isoforms linked to ISPA-28-insensitive channels; cells expressing Dd2 *clag3.1* survive this treatment, as sorbitol uptake is blocked by the inhibitor (4). The reverse selection, which eliminates Dd2 *clag3.1*-expressing cells, was achieved through cultivation with ISPA-28 in a modified culture medium termed PGIM (PSAC growth inhibition medium); PGIM is based on the standard RPMI 1640 formulation but contains lower, more physiological levels of three key nutrients (5). Under these conditions, cells expressing Dd2 *clag3.1* are killed because ISPA-28 prevents nutrient uptake required for parasite growth.

As *TFLC3* and *miniSOG2* express two *clag3* isoforms without epigenetic control, their cultures do not contain subpopulations amenable to purifying selections. We initially predicted that they would therefore not tolerate stringent selections with ISPA-28 because they are constrained to express both sensitive and resistant CLAG3 isoforms simultaneously. We subjected both transfection clones to either the sorbitol or PGIM selection with ISPA-28, observed marked attrition of each culture, and were surprised as resistant mutants were obtained in all four cases (Fig. 5). After limiting dilution cloning, the two mutants obtained after daily sorbitol treatments, called *TFLC3.sorb* and *miniSOG2.sorb*, exhibited significantly improved PSAC block by ISPA-28 ($P \leq 0.001$ for comparisons to unselected merodiploid at a 15 μM concentration; $n = 3$ trials each); inhibition for both selected clones matched the dose responses for wild-type Dd2

FIG 4 Legend (Continued)
using membranes from *miniSOG2* probed with anti-FLAG (E) and anti-CLAG3 (F) antibodies. Proteins were separated after cells were incubated without and with pronase E treatment (− and +, respectively). Both CLAG3 proteins expressed in this parasite are integral to the erythrocyte membrane. (G) ISPA-28 dose responses from experiments as in panel B. Symbols represent mean ± SEM for wild-type parasites (3D7, white circles; Dd2, black circles) and merodiploid transfectants (*TFLC3*, blue triangles; *miniSOG2*, red triangles).

parasites (lower solid line, Fig. 5), suggesting complete loss of the 3D7 CLAG3 protein's contribution to PSAC activity.

The two limiting dilution clones obtained after cultivation in PGIM with ISPA-28, *TFLC3.pgim* and *miniSOG2.pgim*, also relinquished their intermediate phenotypes; both negative-selection clones quantitatively matched the weak ISPA-28 block characteristic of untransfected 3D7 parasites (upper line, Fig. 5).

Because these changes were unexpected, we explored the possible molecular mechanisms. PCR and DNA sequencing revealed that *TFLC3* survived our *in vitro* selections through growth of two distinct transfection revertants. The *TFLC3.pgim* clone underwent ectopic recombination to loop out both the pCC1-attB-Dd2sLE and pLN-attP-Dd2nLE-3D7FL plasmids, presumably as a single 21.6-kb concatemer carrying both the *attL* and *attR* sites (Fig. 6A and S6); DNA sequencing of the *clag3* locus did not reveal any differences relative to the untransfected KC5 parent, suggesting homologous recombination between the identical upstream *clag3* sequences (gray elements at the two ends of the *TFLC3* ribbon schematic, Fig. 1A).

Although integrase-mediated recombination between *attB* and *attP* sites is generally considered irreversible (26), PCR revealed that *TFLC3.sorb* attained high ISPA-28 affinity by looping out only the pLN-attP-Dd2nLE-3D7FL plasmid (Fig. 6A and S6). DNA sequencing revealed full restoration of the gene's last intron and *attB* site without modification, identical to its *C3attB* parent.

Despite exhibiting quantitatively identical changes in PSAC pharmacology, selections applied to the *miniSOG2* merodiploid resulted from distinct molecular changes. Because it carries the Dd2 genetic background, the *miniSOG2* parasite has three *clag3* genes: the *clag3.1* and *clag3.2* genes native to Dd2 as well as the epitope-tagged *clag3.1* of 3D7 introduced through transfection (Fig. 6B). To examine possible contributions from each gene, we began with real-time quantitative PCR (qRT-PCR). As observed with its Dd2 parent (4), *miniSOG2* preferentially expressed the Dd2 *clag3.1* gene, maintaining the native *clag3.2* in a silenced state. Selection with PGIM and ISPA-28 largely reversed this preference (Fig. 6C, red bars showing a 40-fold-reduced expression of the Dd2 *clag3.1* and a 7-fold increase for Dd2 *clag3.2*); these changes can account for the loss in ISPA-28 block and permit growth of *miniSOG2.pgim* despite restricted nutrient access. The 3D7 *clag3.1* transgene did not exhibit altered expression, consistent with its expression under the *msp2* promoter incapable of epigenetic upregulation.

As qRT-PCR did not reveal changes in the *miniSOG2.sorb* parasite (Fig. 6C, blue bars), we next used immunoblotting and found that the FLAG-tagged transgene product was rendered undetectable upon selection for improved ISPA-28 block (Fig. 6D). Immunoblotting with anti-CLAG3 revealed the native Dd2 CLAG3.1 protein (Fig. 6E); the observed faster migration of CLAG3 in *miniSOG2.sorb* than in *miniSOG2.pgim* is consistent with a lower molecular weight of this allele than that of the epitope-tagged 3D7 CLAG3.1 (Fig. 6B). DNA sequencing of the 3D7 transgene revealed a nonsynonymous point mutation that changes glutamine 271 to a stop (Fig. 6F), yielding a truncated 31-kDa protein not detectable by antibodies that recognize downstream epitopes. Thus, both increased and reduced ISPA-28 affinity were obtained through selections applied to the *TFLC3* and *miniSOG2* merodiploids. The parasite may also use other mechanisms, such as increases in *clag3* copy number (5), to survive selections that target this essential nutrient uptake channel.

DISCUSSION

CLAG3 was identified as a critical determinant of infected-cell nutrient uptake through classical genetic mapping with ISPA-28, an isolate-specific PSAC inhibitor found through high-throughput screening (4). While DNA transfections, transport mutants, and functional proteolysis of channel-mediated uptake have provided independent evidence for CLAG3 involvement (6, 7, 9, 14), exactly how this protein contributes to channel activity is unclear. As CLAG3 localizes to the host membrane, either it may directly contribute to pore formation or it may function as a modulator

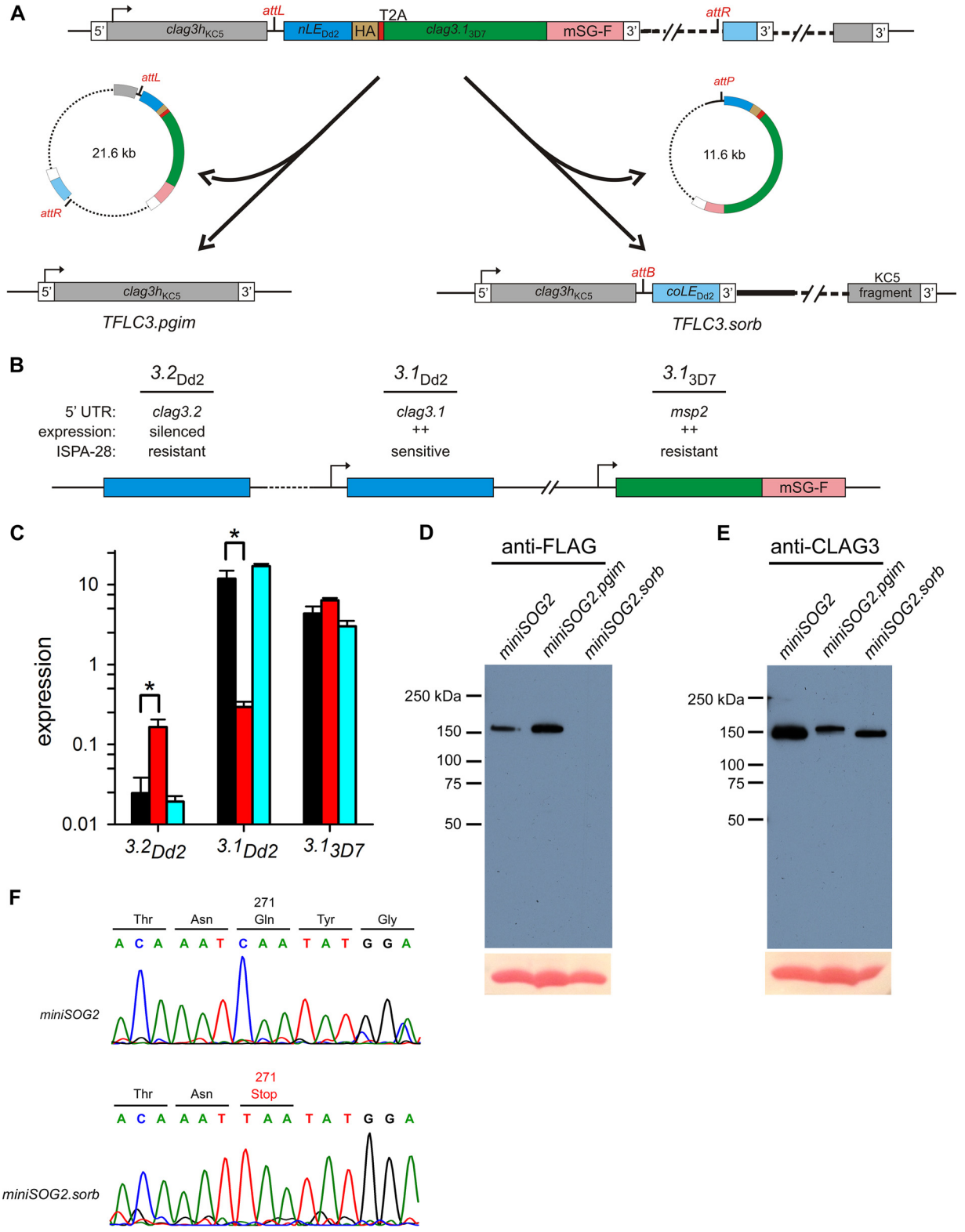

FIG 6 Changes in CLAG3 expression account for observed selection phenotypes. (A) Schematic showing genomic changes upon selection of *TFLC3* to yield the *TFLC3.pgim* and *TFLC3.sorb* clones. These clones loop out one or both transfection plasmids to lose their intermediate channel phenotypes. (B) Schematic showing the three *clag3* genes present in the *miniSOG2* line; the 3D7 *clag3.1* gene is expressed from a distinct genomic site through random *piggyBac* insertion. Distinguishing features of each allele are tabulated above the ribbon. (C) Mean ± SEM normalized expression of indicated *clag3* alleles in the *miniSOG2* line before (black bars) and after selection with ISPA-28 and PGIM or sorbitol (red and blue bars, respectively). *, significant changes in gene expression ($P < 0.05$, one-way ANOVA followed by Dunnett's multiple-comparison test; replicates from 3 independent trials). (D and E) Immunoblot assays using cell lysates from indicated parasites, probed with anti-FLAG (D) or anti-CLAG3 (E) antibodies. (F) DNA sequence chromatograms showing a C-to-T point mutation that changes glutamine 271 to a stop in the *miniSOG2.sorb* parasite.

that activates solute uptake through other pore-forming proteins (3). To explore these and other possible mechanisms, we used a novel transfection approach to produce parasites expressing two distinct CLAG3 paralogs with separate epitope tags. This *TFLC3* transfectant and a separate *miniSOG2* transfectant expressing these two paralogs under separate promoters show that CLAG3 can traffic normally to the host membrane when expression is driven under the *msp2* promoter or when two isoforms are produced with an intervening T2A ribosome skip peptide. These fortuitous observations allowed us to determine that CLAG3 oligomerizes within infected cells. Functional studies with these transfectants then revealed that the relative expression of the Dd2 and 3D7 CLAG3 isoforms quantitatively defines PSAC block by the sequence-specific inhibitor ISPA-28. *In vitro* selections for resistance to PSAC-mediated osmotic lysis or blocked nutrient acquisition independently confirm the relationship between CLAG3 sequence and channel phenotype; these selections also revealed the molecular mechanisms available to parasites to evade selective pressures while preserving essential channel-mediated nutrient uptake.

So how does CLAG3 contribute to PSAC formation? Because CLAG3 is integral to the host membrane and has an amphipathic transmembrane domain (9), one model is direct CLAG3 contribution to the nutrient pore. Arguing against this model is the paucity of predicted transmembrane domains: most ion channels require a minimum of 3 to 5 alpha-helices to create a stable aqueous pore (27). Our finding that CLAG3 undergoes self-association provides a conservative explanation for this: higher-order stoichiometries with each monomer providing a pore-lining transmembrane domain could provide the required number of transmembrane domains. Indeed, many ion channels are formed by oligomerization of identical or highly related subunits (28–30). As CLAG3 associates with RhopH2 and RhopH3 to form a stable complex (15, 16, 31), these other proteins may also contribute to the channel and provide additional transmembrane domains (11). This complicated heteromeric arrangement may also account for the many unusual features of this nutrient uptake channel (32, 33).

Further studies will be required to conclusively determine whether the RhopH complex forms the nutrient pore directly. While heterologous expression could resolve this, the member proteins are large and do not express well in standard expression systems. This endeavor will be further complicated by required cotranslational assembly of the three-protein complex, proteolytic processing of RhopH3 that may be necessary for activation of the pore, and complex trafficking and eventual insertion at the host membrane (11). As CLAG3 must transition from peripheral association with membranes to an integral form at the host cell surface to contribute to PSAC formation (14), each of these steps may require parasite-specific proteases and chaperones that are absent from heterologous expression systems.

Our findings suggest a higher-order stoichiometry to the RhopH complex, with at least two CLAG3 monomers in association with an unknown number of RhopH2 and RhopH3 proteins. Native PAGE, a method that could in principle determine the precise subunit stoichiometry (34), unfortunately cannot be used with confidence here. We determined that these proteins exhibit anomalous migration: under conditions that dissociate the complex and impose migration as monomers, native PAGE overestimates the molecular weights of both CLAG3 and RhopH3 monomers (see Fig. S5 in the supplemental material). As incomplete cleavage of the T2A skip peptide between CLAG3 monomers in *TFLC3* might yield higher-than-expected molecular weights, our native PAGE experiments were performed exclusively with HB3^{3rec}, a transfectant line that expresses a single CLAG3 isoform and does not utilize skip peptides. While the reasons for anomalous migration are unclear, a survey of membrane proteins revealed that a 2-fold-increased apparent molecular weight could be attributed to Coomassie blue binding during migration in native PAGE (35); the same study found substantial effects of detergent choice also. In the case of CLAG3, the apparent molecular weight may also be affected by this protein's highly charged C terminus (36). Another important question is whether this complex also contains CLAG paralogs from other chromosomes (termed CLAG2, CLAG8, and CLAG9). A previous study found that immuno-

precipitation with CLAG9-specific antibody does not pull down either CLAG3 or CLAG2 (10), but the subsequent determination that these proteins are integral to membranes and that the complex is unstable in some detergents requires cautious interpretation of early findings.

The low levels of CLAG3 self-association identified by these coimmunoprecipitation experiments may result from several factors. Because trophozoite-stage immunofluorescence assays (IFAs) and protease susceptibility studies reveal that a small fraction of CLAG3 is successfully delivered and integrated at the host membrane (e.g., Fig. 2), one explanation is that the intracellular pools may be present as monomers and that CLAG3 oligomerization occurs shortly before or upon insertion at the host membrane, a model with good precedent (37). Another possibility is that solubilization with detergents and available coimmunoprecipitation procedures, despite our efforts to optimize these steps, may compromise RhopH complex integrity and underestimate CLAG3 oligomerization (Fig. S5). Yet another consideration is whether the two CLAG3 isoforms that we used, derived from the *clag3.1* products of Dd2 and 3D7 parasites, associate with each other randomly; if these proteins preferentially self-associate, our approach would again underestimate CLAG3 oligomerization. Despite these uncertainties, our reverse immunoprecipitations with two negative-control transfectants suggest that the observed low levels of oligomerization do not represent an experimental artifact.

While the model of CLAG3 oligomerization is appealing, many important questions remain. Because the quantitative correlations that we found between CLAG3 sequence and channel phenotype could also be observed with channels that contain only CLAG3 monomers, we cannot conclusively assign a role to the identified oligomers. Because the measured oligomerization is low relative to the total cellular pool, our various transfectant lines and biochemical studies could also not address whether the CLAG3 oligomers remain associated with RhopH2 and RhopH3, proteins additionally linked to PSAC formation (11). If the resulting heteromeric complex does form the channel, the absolute stoichiometries and functional contributions to pore formation will require exploration for each subunit. Definitive resolution of these uncertainties will require a combination of molecular, structural, and biochemical studies. The large size of RhopH member proteins, epigenetic regulation of *clag* paralogs, and compensatory changes in the parasite genome upon DNA transfection should all be considered carefully in these studies.

From the perspective of host-pathogen interactions, our study provides insights into genome-level changes available to parasites when subjected to strong selective pressures such as osmotic destabilization or target-specific drugs. Based on prior selections targeting PSAC (5), we initially predicted that small-volume cultures of either *TFLC3* or *miniSOG2* would be unable to survive selection either for or against ISPA-28-mediated block because our transfections imposed intermediate ISPA-28 affinity through forced coexpression of two alleles. In contrast to our predictions, both clones rapidly acquired genome-level changes that conferred a quantitatively complete change in ISPA-28 affinity and allowed mutant progeny expansion. We identified epigenetic silencing of the native Dd2 allele, truncation of the 3D7 allele, and loop-out of *attB* and/or *attP* plasmids as strategies available to the parasite.

The loop-out of the *attP* plasmid alone, as observed when *TFLC3* was pressured to increase ISPA-28 block of sorbitol uptake (Fig. 6A and S6), may be the most surprising of these rapidly acquired genome-level changes. This loop-out corresponds to recombination between the *attL* and *attR* sites and is the reverse of the *attB-attP* recombination mediated by Bxb1 integrase. As Bxb1 integrase is generally considered incapable of this reverse reaction in isolation (26), we used PCR to determine that the *TFLC3* clone no longer carries the pINT helper plasmid encoding the integrase. Diagnostic PCR also excluded low-level retention of parasites that failed to integrate the *attP* plasmid in the *TFLC3* limiting dilution clone (lane 4, Fig. S6B). A more likely scenario is that the *attP* plasmid was removed through an alternative form of nonhomologous end joining after a coincidental genome break. Although canonical nonhomologous end joining is not thought to occur in *P. falciparum* due to lack of critical enzymes (38), some alternative mechanisms that utilize very short regions of homology termed "microhomologies"

have been observed infrequently (39, 40). While such mechanisms are typically associated with a residual indel or inversion (41), we could not identify any CLAG3 sequence differences between this selected mutant and the original *C3attB* clone, implicating a clean loop-out of the *attP* transfection plasmid.

Allelic exchange transfection via a silent *attB* site engineered into a gene's intron, as we demonstrate here, represents a useful tool for molecular and cellular studies of gene function. While similar introduction of *loxP* sites into an intron has been used in parasite transfections (42), the present approach is more versatile as a single initial transfection to engineer the silent *attB* enables the full range of downstream modifications—gene truncation, epitope tagging, and insertional and site-directed mutagenesis. While CRISPR-Cas9 transfection will be the method of choice for most gene editing experiments in *P. falciparum*, it is worth noting that CRISPR may not be ideal for insertion of large sequence elements as it requires homologous recombination on both sides of the insert. Another recently described approach, selection-linked integration (43), should also work for most targets but requires an AT-rich homology arm for upstream recombination; it may also fail for proteins with low or undetectable expression in asexual-stage cultures because it depends on the target gene's promoter to drive selectable marker expression. For cases such as the >5-kb insert that we required to produce *TFLC3* (Fig. 1A), integration distal to an engineered silent *attB* site may be the most robust approach.

MATERIALS AND METHODS

Parasite culture. *P. falciparum* laboratory lines were cultivated at 37°C under 5% O_2, 5% CO_2, 90% N_2 in O^+ human erythrocytes (Interstate Blood Bank) using RPMI 1640 supplemented with 25 mM HEPES, 50 μg/ml hypoxanthine (KD Medical), 0.5% New Zealand (NZ) microbiological bovine serum albumin (BSA) (MP Biomedicals), and 0.23% $NaHCO_3$ (Gibco). PGIM follows the RPMI 1640 formulation but contains reduced concentrations of isoleucine, hypoxanthine, and glutamine (5); this medium was supplemented with HEPES, NZ microbiological BSA, and $NaHCO_3$ as described above.

Plasmid construction and DNA transfection. Plasmids were prepared by standard methods and confirmed by DNA sequencing and restriction digestion. Primers used are tallied in Table S1 in the supplemental material.

The pCC1-120w-attB plasmid was used to introduce a silent *attB* site within the last intron of the KC5 *clag3h* gene by single-crossover homologous recombination. A codon-optimized sequence for the last exon facilitated recombination upstream of the desired *attB* sequence. While the upstream homologous sequence was obtained by PCR amplification from KC5, the last exon's sequence was synthesized from the Dd2 CLAG3.1 sequence (17). Parasite transfection was performed by plasmid electroporation into uninfected erythrocytes prior to addition of trophozoite-infected cells for *in vitro* culture (44). After selection with 2 nM WR99210 (Jacobus), parasite growth was detected with Giemsa-stained slides after ~3 weeks; PCR was then used to detect integration prior to limiting dilution cloning to obtain *C3attB* (45).

The Bxb1 integrase system was used for efficient integration at the engineered *attB* (46); this second transfection utilizes two plasmids. The pLN-*attP* plasmids carry the *attP* site and downstream sequences to be integrated, while the pINT helper plasmid encodes Bxb1 integrase. *C3attB* parasites were transfected with these two plasmids and selected with 2.5 μg/ml blasticidin S and 125 μg/ml G418 (Thermo Fisher). Parasite growth and integration were typically detected in ~3 weeks.

The *piggyBac* method was used to integrate a full-length *clag3.1* gene at a distant genomic site through random insertion at one or more transposon target sites (24). The *clag3.1* gene from the 3D7 parasite, an in-frame tandem miniSOG-FLAG epitope tag, and the *clag3.1* 3′ untranslated region (UTR) were cloned behind the *msp2* promoter. This cassette was inserted into the pXL-BacII-hDHFR vector between the inverted terminal repeats (ITRs), which are recognized by the *piggyBac* transposase. The Dd2 parasite line was transfected with this plasmid and the pHTH helper plasmid encoding *piggyBac* (24). Selection with WR99210 for the hDHFR cassette present between the ITRs yielded a transfection pool that was then cloned to obtain the *miniSOG2* line. Southern blotting was used to evaluate retention of pXL-M2-120w-miniSOG episomes and the number of genomic integration events.

Southern blot hybridization. Genomic DNA was extracted using the Quick-gDNA MiniPrep kit (Zymo Research), digested with indicated enzymes, resolved on an 0.7% agarose gel, acid depurinated, and blotted overnight onto an Amersham Hybond N^+ charged membrane (GE Healthcare). A digoxigenin (DIG)-labeled-DNA probe complementary to *hdhfr* was prepared using primers 5′-ATTTCCAGAGAA TGACCACAAC-3′ and 5′-TTAAGATGGCCTGGGTGATTC-3′ and used to evaluate integration in *miniSOG2*. A separate DIG-labeled DNA probe directed against a conserved region of the *clag3* last exon was prepared with 5′-TTTTTCATGGAACTTGCAAATGGTTTCATGTATGC-3′ and 5′-GACATTTTGTTTTTGAAAGCA TTTTCCATATC-3′. PCR was performed with KC5 genomic DNA, pCC1-120w-attB, and pLN-attP-Dd2nLE-3D7FL as the templates. The amplified probes were mixed at equal concentrations and used; these probes were designed to bind *clag3.1*-like sequences from KC5, Dd2, and 3D7 as well as the codon-optimized fragment present in *C3attB* parasites without recognizing *clag* paralogs from other chromosomes. After prehybridization of cross-linked membrane with DIG-Easy Hyb (Roche), the labeled probe

was added and hybridized overnight at 42°C. The blot was washed with low-stringency buffer (0.1× SSC [1× SSC is 0.15 M NaCl plus 0.015 M sodium citrate]-0.1% SDS) at 50°C and blocked. Probe binding was then detected with antidigoxigenin-alkaline phosphatase (AP) Fab fragments at a dilution of 1:10,000 and CDP-Star substrate (Roche).

***In vitro* selections of parasite transfectants.** Synchronous cultures of transfected parasite lines were subjected to osmotic lysis selection by incubation in 5% sorbitol with 0.6 μM ISPA-28 at room temperature for 30 min on 4 consecutive days with cultivation in standard RPMI 1640-based medium as described previously (4). Subsequent cultivation and limiting dilution cloning yielded the *TFLC3.sorb* and *miniSOG2.sorb* lines.

Reverse selection to reduce ISPA-28 sensitivity was performed by cultivation of synchronous cultures at initial parasitemias of 1 to 2% in PGIM supplemented with 5 μM ISPA-28 continuously for 4 days. The culture was then washed and cultivated in standard medium prior to limiting dilution cloning to obtain *TFLC3.pgim* and *miniSOG2.pgim*.

Healthy parasites could not be identified immediately after completion of each of these selections, but regular microscopic examination revealed recovery after approximately 2 weeks. Lines were cryopreserved shortly thereafter. Selection pools were subjected to initial phenotyping and molecular characterization prior to limiting dilution cloning (45); each limiting dilution clone was phenotypically identical to the corresponding selection pool.

Solute transport measurements. Channel-mediated transport was quantified with a kinetic, transmittance-based assay that tracks osmotic lysis of infected cells in sorbitol, a sugar alcohol with high PSAC permeability (47). Trophozoite-stage-infected erythrocytes were enriched with the Percoll-sorbitol method, washed, and resuspended at 37°C in 280 mM sorbitol, 20 mM Na-HEPES, 0.1 mg/ml bovine serum albumin, pH 7.4, to initiate sorbitol uptake and osmotic lysis; indicated concentrations of ISPA-28 were added without preincubation. Lysis was continuously tracked by measuring transmittance of 700-nm light (DU640 spectrophotometer with Peltier temperature control; Beckman Coulter). Inhibitor dose-response relationships were calculated from the time to a fractional lysis threshold. ISPA-28 dose-response data were fitted to the sum of two Langmuir isotherms with the following equations: $P = a/[1 + (x/b)] + (1 - a)/[1 + (x/c)]$, where P represents the normalized sorbitol permeability in the presence of inhibitor at concentration x and a, b, and c are constants. ISPA-28 block contrasts with that of other potent inhibitors, whose dose responses are adequately fitted by a single Langmuir isotherm (5); this difference corresponds to a lack of saturating block despite use of high ISPA-28 concentrations.

Protease susceptibility and membrane fractionation. Enriched trophozoite-infected erythrocytes were suspended in phosphate-buffered saline (PBS) supplemented with 0.6 mM $CaCl_2$ and 1 mM $MgCl_2$ (PBS2) at 5% hematocrit prior to treatment with 1 mg/ml pronase E (Sigma-Aldrich) for 1 h at 37°C. Protease treatment was terminated by adding an equal volume of ice-cold PBS2 with 2 mM phenylmethylsulfonyl fluoride (PMSF) and 2 mM EDTA. After extensive washing with PBS2, the treated cells were lysed in ice-cold hypotonic lysis buffer (7.5 mM $NaHPO_4$, 1 mM EDTA, pH 7.5) with 1 mM PMSF and centrifuged (100,000 × *g*, 4°C, 1 h). The supernatant and pellet were collected as the soluble and membrane fractions. The membrane fraction was then resuspended in 100 mM Na_2CO_3, pH 11, for 30 min on ice before centrifugation (100,000 × *g*, 4°C, 1 h). The resulting supernatant and pellet fractions represent the peripheral and integral membrane protein fractions; both were neutralized with a 1/10 volume of 1 M HCl and solubilized and denatured in Laemmli sample buffer containing 6% SDS.

Coimmunoprecipitation. Enriched trophozoite-infected cells were lysed in 50 mM Tris-HCl (pH 7.4), 150 mM NaCl, 5 mM EDTA with 1% Triton X-100; incubated for 30 min on a shaker at room temperature (RT); and centrifuged (12,000 × *g*, 10 min, 4°C); other detergents were used in place of Triton X-100 as indicated. After reserving an aliquot as the input, the solubilized protein was incubated with washed anti-FLAG or anti-HA affinity agarose beads (Sigma-Aldrich) with gentle mixing for a minimum of 2 h at 4°C. We optimized the ratio of solubilized protein to affinity beads and confirmed complete bait protein binding with control immunoblot assays of the unbound supernatant after this incubation. The resin was then washed 5 times with IP wash buffer (50 mM Tris-HCl, pH 7.4, 50 mM NaCl, 5 mM EDTA) and the corresponding detergent. After an additional wash in SDS-free elution buffer, bound proteins were eluted into 100 mM Tris, pH 6.8, with 4% SDS; elution was also performed using 3× FLAG peptide (Sigma-Aldrich) in some experiments. After electrophoresis, proteins were evaluated by immunoblotting or silver staining (Pierce).

Immunoblot assays. Proteins were separated by SDS-PAGE (4 to 15% Mini-Protean TGX gel; Bio-Rad) and transferred to nitrocellulose membrane. After blocking (5% skim milk in PBS), primary antibodies were applied overnight in blocking buffer (anti-CLAG3, 1:2,000 dilution [4]; anti-RhopH3, 1:5,000 [11]; anti-HA tag, 1:1,000 [EMD Millipore]; anti-FLAG M2 monoclonal [1:1,000, Sigma-Aldrich; catalog no. F3165]). After washing, horseradish peroxidase (HRP)-conjugated secondary anti-mouse or anti-rabbit antibodies were applied (1:2,000 to 1:5,000; Sigma-Aldrich) with Clarity Western ECL substrate (Bio-Rad). Bound antibody was detected on Hyblot X-ray film. All immunoblots shown are representative of at least three trials; band intensities were estimated using ImageJ software (https://imagej.nih.gov/).

Blue native PAGE experiments used enriched HB3^{3rec} parasites freeze-thawed into PBS with 1 mM PMSF. The membrane fraction was solubilized in 150 mM NaCl, 10 mM Tris, 1 mM EDTA, pH 7.5, with 1 mM PMSF and indicated detergents at 4°C for 15 min with gentle mixing. After centrifugation at 150,000 × *g* to remove insoluble material, a fraction was treated with 0.1% SDS for 30 min at 4°C to disrupt protein complexes. Native PAGE sample buffer was added to a 1× concentration; Coomassie blue G-250 was then added to 25% of the total detergent concentration prior to electrophoresis at 4°C (native PAGE 4 to 16% Bis-Tris gel; Thermo Fisher). A voltage of 150 V was applied for 30 min with Dark Blue Cathode buffer containing 0.02% Coomassie blue G-250 prior to replacement with Light Blue Cathode

buffer (0.002% Coomassie blue G-250) and resumption of electrophoresis at 150 V for 30 min and 250 V for 60 min based on the manufacturer's recommendations. The gel was then incubated with transfer buffer (25 mM Tris-HCl, 192 mM glycine, 10% methanol, and 0.1% SDS) for 30 min prior to transfer to polyvinylidene difluoride (PVDF) at 150 mA for 90 min. After fixation with 5% acetic acid and Coomassie blue removal with methanol, blots were blocked with 150 mM NaCl, 20 mM Tris-HCl, pH 7.4, and 0.1% Tween 20 with 3% skim milk prior to antibody application and detection as described above.

Immunofluorescence microscopy. Indirect immunofluorescence confocal microscopy was performed with thin smears of parasite cultures. Dried slides were fixed with a chilled 1:1 mixture of acetone and methanol before blocking in 3% skim milk in PBS for 1 h at RT. Slides were then incubated in blocking buffer with indicated primary antibodies at a 1:100 dilution for 1 h at RT (mouse anti-HA [Sigma-Aldrich] and rabbit anti-FLAG [Cell Signaling]). After washing, the slide was incubated with 4′,6-diamidino-2-phenylindole (DAPI) (2 μg/μl) and goat anti-mouse Alexa Fluor 488 or goat anti-rabbit Alexa Fluor 594 (Thermo Fisher) for 30 min at RT. Slides were then washed in ice-cold PBS for 5 min before mounting with ProLong Diamond antifade mountant (Molecular Probes). Images were collected under a 64× oil immersion objective on a Leica SP5 confocal microscope and processed using Leica LAS X software.

qRT-PCR. Normalized expression levels for the three copies of *clag3* in *miniSOG2* parasites before and after *in vitro* selection were measured with real-time PCR. Total RNA was harvested from cultures 27 h after sorbitol synchronization with the Ambion PureLink RNA minikit. Contaminating DNA was removed with RNase-free DNase I (Ambion) prior to first-strand cDNA synthesis using reverse transcription with SuperScript III (Invitrogen), 1.7 μg RNA, and oligo(dT) primers. The constitutively expressed parasite gene PF07_0073 was used for normalization of gene expression among the three examined parasite lines as described previously (6).

Real-time PCR was performed with the synthesized cDNA, primers listed in Table S1 in the supplemental material, and the QuantiTect SYBR Green kit (Qiagen). Primers for real-time quantitative PCR (qRT-PCR) were designed based on specificity for individual *clag3* paralogs and a desired amplicon size of ~120 bp. qRT-PCR was carried out using the iCycler IQ multicolor real-time PCR system (Bio-Rad) according to the following procedure: denaturation at 95°C for 15 min followed by 40 cycles of denaturing at 94°C, annealing at 55°C, and extension at 62°C (30 s each). After cycling, the reaction mixture was gradually heated from 55°C to 95°C in 0.5°C increments over 30 s to confirm the specificity of primer binding and product synthesis. Each qRT-PCR mixture was accompanied by a negative control without reverse transcriptase to exclude genomic DNA contamination. All reactions were performed in triplicate wells for each of three separate harvests. The average threshold cycle (C_T) values were used to obtain normalized gene expression according to 2^(mean C_T value of the test *clag3* gene − mean C_T value of Pf07_0073 gene). Expression changes relative to the *miniSOG2* parent were calculated with the $2^{-\Delta\Delta CT}$ method (48).

Statistical analysis. Numerical data are presented as mean ± standard error of the mean (SEM). Statistical significance was determined with the unpaired Student *t* test or one-way analysis of variance (ANOVA) with Dunnett's multiple-comparison *post hoc* analysis. A threshold of $P < 0.05$ was used for significance.

SUPPLEMENTAL MATERIAL

Supplemental material for this article may be found at https://doi.org/10.1128/mBio.02293-17.

FIG S1, PDF file, 0.1 MB.
FIG S2, TIF file, 2.2 MB.
FIG S3, TIF file, 0.6 MB.
FIG S4, TIF file, 2 MB.
FIG S5, JPG file, 0.7 MB.
FIG S6, TIF file, 2.3 MB.
TABLE S1, XLSX file, 0.02 MB.

ACKNOWLEDGMENTS

We thank Kristen Lane for technical guidance on Southern blotting and qRT-PCR and Jacquin Niles, Ganesan Suresh, and Nasamu Sebastian for help with production of the Bac-TetR-*clag3.1*-10xApt plasmid.

This study was supported by the Intramural Research Program of the National Institutes of Health, National Institute of Allergy and Infectious Diseases. The funders had no role in study design, data collection and analysis, decision to publish, or preparation of the manuscript.

REFERENCES

1. Maier AG, Cooke BM, Cowman AF, Tilley L. 2009. Malaria parasite proteins that remodel the host erythrocyte. Nat Rev Microbiol 7:341–354. https://doi.org/10.1038/nrmicro2110.
2. Hviid L, Jensen AT. 2015. PfEMP1—a parasite protein family of key importance in *Plasmodium falciparum* malaria immunity and pathogenesis. Adv Parasitol 88:51–84. https://doi.org/10.1016/bs.apar.2015.02.004.

3. Desai SA. 2012. Ion and nutrient uptake by malaria parasite-infected erythrocytes. Cell Microbiol 14:1003–1009. https://doi.org/10.1111/j.1462-5822.2012.01790.x.
4. Nguitragool W, Bokhari AA, Pillai AD, Rayavara K, Sharma P, Turpin B, Aravind L, Desai SA. 2011. Malaria parasite *clag3* genes determine channel-mediated nutrient uptake by infected red blood cells. Cell 145:665–677. https://doi.org/10.1016/j.cell.2011.05.002.
5. Pillai AD, Nguitragool W, Lyko B, Dolinta K, Butler MM, Nguyen ST, Peet NP, Bowlin TL, Desai SA. 2012. Solute restriction reveals an essential role for *clag3*-associated channels in malaria parasite nutrient acquisition. Mol Pharmacol 82:1104–1114. https://doi.org/10.1124/mol.112.081224.
6. Sharma P, Wollenberg K, Sellers M, Zainabadi K, Galinsky K, Moss E, Nguitragool W, Neafsey D, Desai SA. 2013. An epigenetic antimalarial resistance mechanism involving parasite genes linked to nutrient uptake. J Biol Chem 288:19429–19440. https://doi.org/10.1074/jbc.M113.468371.
7. Mira-Martínez S, Rovira-Graells N, Crowley VM, Altenhofen LM, Llinás M, Cortés A. 2013. Epigenetic switches in *clag3* genes mediate blasticidin S resistance in malaria parasites. Cell Microbiol 15:1913–1923. https://doi.org/10.1111/cmi.12162.
8. Rovira-Graells N, Crowley VM, Bancells C, Mira-Martínez S, Ribas de Pouplana L, Cortés A. 2015. Deciphering the principles that govern mutually exclusive expression of *Plasmodium falciparum clag3* genes. Nucleic Acids Res 43:8243–8257. https://doi.org/10.1093/nar/gkv730.
9. Sharma P, Rayavara K, Ito D, Basore K, Desai SA. 2015. A CLAG3 mutation in an amphipathic transmembrane domain alters malaria parasite nutrient channels and confers leupeptin resistance. Infect Immun 83:2566–2574. https://doi.org/10.1128/IAI.02966-14.
10. Kaneko O, Yim Lim BYS, Iriko H, Ling IT, Otsuki H, Grainger M, Tsuboi T, Adams JH, Mattei D, Holder AA, Torii M. 2005. Apical expression of three RhopH1/Clag proteins as components of the *Plasmodium falciparum* RhopH complex. Mol Biochem Parasitol 143:20–28. https://doi.org/10.1016/j.molbiopara.2005.05.003.
11. Ito D, Schureck MA, Desai SA. 2017. An essential dual-function complex mediates erythrocyte invasion and channel-mediated nutrient uptake in malaria parasites. Elife 6:e23485. https://doi.org/10.7554/eLife.23485.
12. Sherling ES, Knuepfer E, Brzostowski JA, Miller LH, Blackman MJ, van Ooij C. 2017. The *Plasmodium falciparum* rhoptry protein RhopH3 plays essential roles in host cell invasion and nutrient uptake. Elife 6:e23239. https://doi.org/10.7554/eLife.23239.
13. Counihan NA, Chisholm SA, Bullen HE, Srivastava A, Sanders PR, Jonsdottir TK, Weiss GE, Ghosh S, Crabb BS, Creek DJ, Gilson PR, de Koning-Ward TF. 2017. *Plasmodium falciparum* parasites deploy RhopH2 into the host erythrocyte to obtain nutrients, grow and replicate. Elife 6:e23217. https://doi.org/10.7554/eLife.23217.
14. Nguitragool W, Rayavara K, Desai SA. 2014. Proteolysis at a specific extracellular residue implicates integral membrane CLAG3 in malaria parasite nutrient channels. PLoS One 9:e93759. https://doi.org/10.1371/journal.pone.0093759.
15. Cortés A, Carret C, Kaneko O, Yim Lim BY, Ivens A, Holder AA. 2007. Epigenetic silencing of *Plasmodium falciparum* genes linked to erythrocyte invasion. PLoS Pathog 3:e107. https://doi.org/10.1371/journal.ppat.0030107.
16. Gupta A, Thiruvengadam G, Desai SA. 2015. The conserved *clag* multigene family of malaria parasites: essential roles in host-pathogen interaction. Drug Resist Updat 18:47–54. https://doi.org/10.1016/j.drup.2014.10.004.
17. Iriko H, Kaneko O, Otsuki H, Tsuboi T, Su XZ, Tanabe K, Torii M. 2008. Diversity and evolution of the *rhoph1/clag* multigene family of *Plasmodium falciparum*. Mol Biochem Parasitol 158:11–21. https://doi.org/10.1016/j.molbiopara.2007.11.004.
18. Shu X, Lev-Ram V, Deerinck TJ, Qi Y, Ramko EB, Davidson MW, Jin Y, Ellisman MH, Tsien RY. 2011. A genetically encoded tag for correlated light and electron microscopy of intact cells, tissues, and organisms. PLoS Biol 9:e1001041. https://doi.org/10.1371/journal.pbio.1001041.
19. Kim JH, Lee SR, Li LH, Park HJ, Park JH, Lee KY, Kim MK, Shin BA, Choi SY. 2011. High cleavage efficiency of a 2A peptide derived from porcine teschovirus-1 in human cell lines, zebrafish and mice. PLoS One 6:e18556. https://doi.org/10.1371/journal.pone.0018556.
20. Kaneko O. 2007. Erythrocyte invasion: vocabulary and grammar of the Plasmodium rhoptry. Parasitol Int 56:255–262. https://doi.org/10.1016/j.parint.2007.05.003.
21. Beck JR, Muralidharan V, Oksman A, Goldberg DE. 2014. PTEX component HSP101 mediates export of diverse malaria effectors into host erythrocytes. Nature 511:592–595. https://doi.org/10.1038/nature13574.
22. Crichton PG, Harding M, Ruprecht JJ, Lee Y, Kunji ER. 2013. Lipid, detergent, and Coomassie blue G-250 affect the migration of small membrane proteins in blue native gels: mitochondrial carriers migrate as monomers not dimers. J Biol Chem 288:22163–22173. https://doi.org/10.1074/jbc.M113.484329.
23. Zainabadi K. 2016. Malaria parasite CLAG3, a protein linked to nutrient channels, participates in high molecular weight membrane-associated complexes in the infected erythrocyte. PLoS One 11:e0157390. https://doi.org/10.1371/journal.pone.0157390.
24. Balu B, Shoue DA, Fraser MJ, Jr, Adams JH. 2005. High-efficiency transformation of *Plasmodium falciparum* by the lepidopteran transposable element *piggyBac*. Proc Natl Acad Sci U S A 102:16391–16396. https://doi.org/10.1073/pnas.0504679102.
25. Wickham ME, Thompson JK, Cowman AF. 2003. Characterisation of the merozoite surface protein-2 promoter using stable and transient transfection in *Plasmodium falciparum*. Mol Biochem Parasitol 129:147–156. https://doi.org/10.1016/S0166-6851(03)00118-X.
26. Ghosh P, Wasil LR, Hatfull GF. 2006. Control of phage Bxb1 excision by a novel recombination directionality factor. PLoS Biol 4:e186. https://doi.org/10.1371/journal.pbio.0040186.
27. Oiki S, Madison V, Montal M. 1990. Bundles of amphipathic transmembrane alpha-helices as a structural motif for ion-conducting channel proteins: studies on sodium channels and acetylcholine receptors. Proteins 8:226–236. https://doi.org/10.1002/prot.340080305.
28. Alam A, Jiang Y. 2011. Structural studies of ion selectivity in tetrameric cation channels. J Gen Physiol 137:397–403. https://doi.org/10.1085/jgp.201010546.
29. Sine SM. 2012. End-plate acetylcholine receptor: structure, mechanism, pharmacology, and disease. Physiol Rev 92:1189–1234. https://doi.org/10.1152/physrev.00015.2011.
30. Goetz T, Arslan A, Wisden W, Wulff P. 2007. GABA(A) receptors: structure and function in the basal ganglia. Prog Brain Res 160:21–41. https://doi.org/10.1016/S0079-6123(06)60003-4.
31. Kaneko O, Tsuboi T, Ling IT, Howell S, Shirano M, Tachibana M, Cao YM, Holder AA, Torii M. 2001. The high molecular mass rhoptry protein, RhopH1, is encoded by members of the *clag* multigene family in *Plasmodium falciparum* and *Plasmodium yoelii*. Mol Biochem Parasitol 118:223–231. https://doi.org/10.1016/S0166-6851(01)00391-7.
32. Bokhari AA, Solomon T, Desai SA. 2008. Two distinct mechanisms of transport through the plasmodial surface anion channel. J Membr Biol 226:27–34. https://doi.org/10.1007/s00232-008-9136-2.
33. Desai SA. 2005. Open and closed states of the plasmodial surface anion channel. Nanomedicine 1:58–66. https://doi.org/10.1016/j.nano.2004.11.001.
34. Wittig I, Braun HP, Schägger H. 2006. Blue native PAGE. Nat Protoc 1:418–428. https://doi.org/10.1038/nprot.2006.62.
35. Heuberger EH, Veenhoff LM, Duurkens RH, Friesen RH, Poolman B. 2002. Oligomeric state of membrane transport proteins analyzed with blue native electrophoresis and analytical ultracentrifugation. J Mol Biol 317:591–600. https://doi.org/10.1006/jmbi.2002.5416.
36. Alkhalil A, Hong L, Nguitragool W, Desai SA. 2012. Voltage-dependent inactivation of the plasmodial surface anion channel via a cleavable cytoplasmic component. Biochim Biophys Acta 1818:367–374. https://doi.org/10.1016/j.bbamem.2011.11.010.
37. Wang JM, Zhang L, Yao Y, Viroonchatapan N, Rothe E, Wang ZZ. 2002. A transmembrane motif governs the surface trafficking of nicotinic acetylcholine receptors. Nat Neurosci 5:963–970. https://doi.org/10.1038/nn918.
38. Lee AH, Symington LS, Fidock DA. 2014. DNA repair mechanisms and their biological roles in the malaria parasite *Plasmodium falciparum*. Microbiol Mol Biol Rev 78:469–486. https://doi.org/10.1128/MMBR.00059-13.
39. Kirkman LA, Lawrence EA, Deitsch KW. 2014. Malaria parasites utilize both homologous recombination and alternative end joining pathways to maintain genome integrity. Nucleic Acids Res 42:370–379. https://doi.org/10.1093/nar/gkt881.
40. Singer M, Marshall J, Heiss K, Mair GR, Grimm D, Mueller AK, Frischknecht F. 2015. Zinc finger nuclease-based double-strand breaks attenuate malaria parasites and reveal rare microhomology-mediated end joining. Genome Biol 16:249. https://doi.org/10.1186/s13059-015-0811-1.
41. Sfeir A, Symington LS. 2015. Microhomology-mediated end joining: a back-up survival mechanism or dedicated pathway? Trends Biochem Sci 40:701–714. https://doi.org/10.1016/j.tibs.2015.08.006.

42. Jones ML, Das S, Belda H, Collins CR, Blackman MJ, Treeck M. 2016. A versatile strategy for rapid conditional genome engineering using loxP sites in a small synthetic intron in *Plasmodium falciparum*. Sci Rep 6:21800. https://doi.org/10.1038/srep21800.
43. Birnbaum J, Flemming S, Reichard N, Soares AB, Mesén-Ramírez P, Jonscher E, Bergmann B, Spielmann T. 2017. A genetic system to study *Plasmodium falciparum* protein function. Nat Methods 14:450–456. https://doi.org/10.1038/nmeth.4223.
44. Deitsch K, Driskill C, Wellems T. 2001. Transformation of malaria parasites by the spontaneous uptake and expression of DNA from human erythrocytes. Nucleic Acids Res 29:850–853. https://doi.org/10.1093/nar/29.3.850.
45. Lyko B, Hammershaimb EA, Nguitragool W, Wellems TE, Desai SA. 2012. A high-throughput method to detect *Plasmodium falciparum* clones in limiting dilution microplates. Malar J 11:124. https://doi.org/10.1186/1475-2875-11-124.
46. Nkrumah LJ, Muhle RA, Moura PA, Ghosh P, Hatfull GF, Jacobs WR, Jr, Fidock DA. 2006. Efficient site-specific integration in *Plasmodium falciparum* chromosomes mediated by mycobacteriophage Bxb1 integrase. Nat Methods 3:615–621. https://doi.org/10.1038/nmeth904.
47. Pillai AD, Pain M, Solomon T, Bokhari AA, Desai SA. 2010. A cell-based high-throughput screen validates the plasmodial surface anion channel as an antimalarial target. Mol Pharmacol 77:724–733. https://doi.org/10.1124/mol.109.062711.
48. Livak KJ, Schmittgen TD. 2001. Analysis of relative gene expression data using real-time quantitative PCR and the 2(-delta delta C(T)) method. Methods 25:402–408. https://doi.org/10.1006/meth.2001.1262.